NJC

ROYAL SOCIETY OF CHEMISTRY

PAPER

View Article Online
View Journal | View Issue

Check for updates

Cite this: *New J. Chem.*, 2018, **42**, 18448

Thiophene insertion for continuous modulation of the photoelectronic properties of triphenylamine-based metal–organic frameworks for photocatalytic sulfonylation–cyclisation of activated alkenes†

Tiexin Zhang,‡*[a] Yusheng Shi,‡[a] Sen Zhang,[a] Chen Jia,[a] Cheng He[a] and Chunying Duan*[ab]

Received 14th August 2018,
Accepted 11th October 2018

DOI: 10.1039/c8nj04151b

rsc.li/njc

Pharmaceutically meaningful conversions like photocatalytic sulfonylation call for the precise control of the photoelectronic properties of photocatalysts. A ligand engineering strategy of inserting different numbers of thiophenes into the scaffold of triphenylamine (**TPA**)-based ligands was developed to improve the visible light absorption, enhance the oxidation potentials of the ground states, and decrease the reduction potentials of the excited states, providing a powerful tool for continuous modulation of the photoelectronic properties of metal–organic framework (MOF)-based heterogeneous photocatalysts. The ligand inserted with two thiophenes was found to possess a well-balanced photoelectronic performance, endowing the corresponding MOF Zn–**BCTA** with good visible light-harvesting ability and a moderate excited-state reduction potential with minimal over-potential for the photoinduced generation of sulfonyl radicals while avoiding the competitive over-reduction of the sulfonyl moieties. The breaking of the C_3-symmetry of the **TPA**-based ligand forged a distorted coordination geometry of the Zn_4O nodes of the MOF to provide potential active sites to facilitate the fixation and activation of α,β-unsaturated carbonyl substrates, and the two-fold interpenetrated frameworks further enhanced the spatial proximity between the encapsulated substrate and the photoredox-active centre. The synergy of the well-tuned photoelectronic properties of Zn–**BCTA** and the spatial confinement effect within the pores benefited the tandem sulfonylation–cyclisation of unsaturated alkenes in an efficient and diastereo-selective mode for the construction of bio-interesting sulphoyl isoquinolinediones/oxindoles.

Introduction

Sulfones are key compounds widely applied in medicines and agricultural chemicals.[1] In comparison to classic sulfa drugs containing easily prepared sulfamides, drugs bearing aryl alkyl sulfone scaffolds such as the antipsychotic medication Amisulpride (also known as Solian®) are more challenging to access and multistep syntheses,[2] hypertoxic reagents,[3] and poor functional group tolerances are generally encountered during the introduction of the sulfone moiety. Comparatively, the addition of aryl sulfonyl radicals with alkenes provides a facile route for the preparation of aryl alkyl sulfones with excellent functional group tolerance.[4] Moreover, photoredox catalysis was recently employed for the generation of aryl sulfonyl radicals,[5–7] avoiding the use of harmful radical initiators[8] and showing potential for improving pharmaceutical technology with clean photoenergy. Bearing in mind the use of expensive, toxic, and irrecoverable polypyridyl noble metal complexes as the photocatalysts in the reported procedures, it is highly desirable to develop the arylsulfonylation of alkenes in the presence of heterogeneous photocatalysts constructed from more economic and less harmful organic dyes. It should be noted that the electrochemical demands on arylsulfonyl chlorides for the generation of aryl sulfonyl radicals raise the requirements for the specific photoelectronic performance of the photocatalyst. First, the reduction potential of the excited state of the photocatalyst should cover the diverse range of electronically differentiated sulfonyl chlorides ($E_{1/2}$ = −0.44 to −1.39 V *vs.* SCE).[9,10] More importantly,

---

[a] *State Key Laboratory of Fine Chemicals, Dalian University of Technology, Dalian 116024, China. E-mail: zhangtiexin@dlut.edu.cn, cyduan@dlut.edu.cn; Fax: +86-411-84986476; Tel: +86-411-84986476*

[b] *Collaborative Innovation Center of Chemical Science and Engineering, Tianjin 300071, China*

† Electronic supplementary information (ESI) available. CCDC 1861320. For ESI and crystallographic data in CIF or other electronic format see DOI: 10.1039/c8nj04151b

‡ T. Zhang and Y. Shi contributed equally to this work.

the competitive reduction of the sulfonyl moiety[11] *vs.* the desired bond dissociation of S–Cl under an over-negative electronic potential implies that the over-potential of the reduction potential of the excited state should be as small as possible. Moreover, the use of lower energy visible light is strongly recommended to avoid background reactions and the other destructive pathways caused by the higher energy UV region.

As inorganic–organic composite materials, metal–organic frameworks (MOFs) feature the advantages of both heterogeneous inorganic molecular sieves and homogeneous organic unimolecules,[12,13] and the tenability and flexibility of MOFs allow for the uniform incorporation of photoactive organic dyes in high densities around the pores,[14–17] and the tuning of the photoelectronic performance of the framework through ligand engineering.[18,19] To achieve precise control of the shifting energy levels of the ground and excited states and the enhancement of the visible light harvesting ability of MOFs, continuous structural modulation of a dye-based ligand scaffold is highly desirable, however, it is still in its infancy. A well-known photoresponsive triphenylamine-based ligand, H_3**TCA** (4,4′,4″-tricarboxyltriphenylamine, with UV-vis absorption λ_{max} = *ca.* 350 nm, and a reduction potential of the excited state of *ca.* −2.20 V) has been successfully incorporated into MOFs[20] for photocatalytic organic transformations,[21] and its three aryl moieties with their C_3-symmetry provide potential sites for iterative decoration to achieve continuous modulation of the photoelectronic properties. The widely applied modulation method of appending electron-donating groups such as amino/alkyl amino groups[22] should be excluded since those groups are not compatible with the sulfonyl radical precursor sulfonyl chlorides and the lone pair electrons of the *N*-containing groups might disturb the photoredox cycle. Thus, inserting an electron-rich aromatic moiety like thiophene into the scaffold of H_3**TCA** to enlarge the π-system is expected to be more practical. Herein, we report a ligand engineering strategy of iterative thiophene insertion for continuous modulation of the photoelectronic properties of triphenylamine-based metal–organic frameworks, with the aim of fine-tuning the photocatalytic sulfonylation of alkenes.

Experimental section

Materials and methods

Unless otherwise stated, organic solvents were dried and distilled prior to use in accordance with standard methods. The other commercially available chemicals were of reagent-grade quality, and were used as received. TLC was carried out on SiO_2 (silica gel 60 F254, Merck), and the spots were located with UV light. Flash chromatography was carried out on SiO_2 (silica gel, 200–300 mesh).

NMR spectra were measured on Bruker Avance 500 WB and Bruker Avance 400 WB spectrometers, and chemical shifts were recorded in parts per million (ppm, δ). Elemental analysis was conducted on a Vario EL III elemental analyzer. High resolution mass spectra were recorded on a LC/Q-TOF mass spectrometer (Micromass, England) equipped with a Z-spray ionization source.

Thermogravimetric analysis (TGA) was carried out with a Mettler-Toledo TGA/SDTA851 instrument. Powder X-ray diffraction (PXRD) measurements were performed with a PANalytical Empyrean X-ray powder diffractometer (Cu Kα radiation, 40 kV, 40 mA). FT-IR spectra were measured as KBr pellets on a JASCO FT/IR-430. Solid and liquid UV-vis spectra were recorded on a Hitachi U-4100 UV-vis-NIR spectrophotometer and a TU-1900 spectrophotometer, respectively.

Solid state cyclic voltammograms were obtained using a carbon-paste working electrode; a well-ground mixture of each bulk sample and carbon paste (graphite and mineral oil) was set in the channel of a glass tube and connected to a copper wire. A platinum-wire counter electrode and an Ag/AgCl reference electrode were utilized. Measurements were conducted using a three-electrode system in an acetonitrile solution of ammonium hexafluorophosphate (0.1 M) at a scan rate of 100 mV s^{-1}.

Solid and liquid fluorescence spectra were measured on an Edinburgh FS920 instrument. The excitation and emission slits were both 3 nm wide, and the wavelengths of excitation and emission were chosen according to each specific case. Time-resolved luminescence spectra were measured with an Edinburgh FLS920 spectrometer.

Synthetic procedures

Synthesis and characterization of ligand H_3BCTA, 2. Br_2 (1.7 mL, 33.18 mmol) was added dropwise to a solution of NaOH (3.9 g, 97.51 mmol) in water (16 mL) in an ice bath, the mixture was further stirred for 20 min, then it was transferred to a constant pressure funnel and added dropwise to a solution of 1,1′-((((4-acetylphenyl)azanediyl)bis(4,1-phenylene))bis(thiophene-5,2-diyl))bis(ethan-1-one) (1.61 g, 3.00 mmol) in 1,4-dioxane (30 mL). The reaction mixture was heated at 45 °C for 5 h, and after that it was put in an ice bath and an aqueous solution of saturated hydroxylamine HCl was added to deoxidize excessive sodium hypobromite. The solution was acidified with diluted hydrochloric acid and the precipitated solid was filtered and recrystallized from acetic acid to afford the pure product (1.48 g, 91%). ^1H NMR (400 MHz, DMSO-d_6) δ 12.32 (br s, 3H), 7.87 (d, *J* = 8.6 Hz, 2H), 7.75 (d, *J* = 8.5 Hz, 4H), 7.70 (d, *J* = 3.8 Hz, 2H), 7.53 (d, *J* = 3.8 Hz, 2H), 7.17 (d, *J* = 8.5 Hz, 4H) and 7.09 (d, *J* = 8.6 Hz, 2H). ^{13}C NMR (101 MHz, DMSO) δ 166.8, 162.8, 150.2, 149.3, 146.4, 134.4, 132.8, 131.0, 128.7, 127.4, 125.4, 124.4, 124.2 and 121.6. FTIR (KBr pellet; cm^{-1}): 3269, 2675, 2549, 1677, 1594, 1536, 1508, 1448, 1320, 1275, 1178, 1104, 810 and 752 cm^{-1}. HRMS (ESI) *m/z* calcd for $C_{29}H_{19}NO_6S_2$ [M^+] 541.0654, found 541.0658.

Mono[4-(5-carboxy-2-thienyl)phenyl]bis(4-carboxyphenyl) amine (H_3**MCTA, 1**) and tris[4-(5-carboxy-2-thienyl)phenyl] amine (H_3**TCTA, 3**)[23] were prepared using similar procedures to that of H_3**BCTA, 2.** See the ESI† section for details.

Synthesis of Zn–BCTA. A mixture of H_3**BCTA** (8.1 mg, 0.015 mmol) and $Zn(NO_3)_2\cdot 6H_2O$ (29.7 mg, 0.1 mmol) was dissolved in 3 mL of DMF in a Teflon-lined steel autoclave and then HOAc (10 μL) was added. The autoclave was sealed and the resulting mixture was kept in an oven at 100 °C for 3 days. The block yellow crystals for X-ray structural analysis were collected by filtration. Yield: 65%. ^{1}H NMR (400 MHz, DMSO-d$_6$/DCl): δ 7.83 (d, J = 8.8 Hz, 2H), 7.70 (d, J = 9.0 Hz, 4H), 7.49 (d, J = 3.9 Hz, 2H), 7.45 (d, J = 4.3 Hz, 2H), 7.12 (d, J = 8.7 Hz, 4H) and 7.06–7.02 (d, J = 8.8 Hz, 2H). Anal. calcd for $(Zn_4O)(C_{29}H_{16}NO_6S_2)_2(C_3H_7NO)_2$ (dried vacuum %): C, 51.22; H, 3.09; N, 3.73; S, 8.55; Found: C, 51.08; H, 3.20; N, 3.87; S, 8.38. IR (KBr): 3036, 1652, 1596, 1558, 1534, 1505, 1446, 1395, 1319, 1288, 1273, 1181, 1110, 1044, 1014, 960, 839 and 815 cm^{-1}.

Single-crystal X-ray crystallography

A single crystal of Zn–**BCTA** with suitable dimensions was selected and placed in a glass tube filled with the mother liquid for data collection. The intensity data for the crystal were collected at 220 K on a Bruker SMART APEX diffractometer equipped with a CCD area detector and a Mo Kα (λ = 0.71073 Å) radiation source.[24] The data integration and reduction were processed using SAINT software.[25] The structure was solved using direct methods and refined on F^2 with the full-matrix least-squares method using the program SHELXL-2017.[26] One of the carbon atoms in coordinated DMF solvent was disordered into two parts with the site occupied factor of each part refined with a free variable value. Except for the disordered carbon atom, all of the non-hydrogen atoms were refined with anisotropic thermal displacement coefficients. The hydrogen atoms were fixed geometrically at calculated positions and allowed to ride on the parent non-hydrogen atoms. To assist the refinements, thermal parameters on adjacent atoms of several benzene and thiophene rings were restrained to be similar. The SQUEEZE routine in PLATON[27,28] was used to deal with the dissociative solvents within the framework and remove their contribution to the overall intensity of the data. Crystallographic data of Zn–**BCTA** are summarized in Table S1 (ESI†).

Dye uptake experiments

Crystals of Zn–**BCTA** (27.1 mg, 18.0 μmol) were soaked in a saturated solution of methylene blue in acetonitrile for 12 h and the resulting crystals were washed with acetonitrile thoroughly till the solution became clear, and then briefly dried on filter paper. The washed samples were digested using minimal amounts of concentrated aqueous HCl and the resultant clear solution was diluted to 500 mL with acetonitrile. The same amount of concentrated aqueous HCl was used when preparing methylene blue solution in acetonitrile with gradient concentrations for the standard curve. The concentration of released methylene blue was determined by comparing the UV-vis absorption to a standard curve (Fig. 3a). The amount of methylene blue taken up by Zn–**BCTA** was calculated to be 14.1 mg (52%, wt%).

General procedure (GP) for photocatalysed tandem sulfonylation–cyclisation with Zn–BCTA

To a pre-dried Pyrex tube equipped with a cooling water system, Zn–**BCTA** crystals (0.00625 mmol), the substrate (0.25 mmol), and TsCl (0.50 mmol) were added. Then the tube was sealed with a rubber septum and subjected to three vacuum/N_2 refill cycles. After adding anhydrous degassed acetonitrile (1 mL) and 2,4,6-collidine (0.50 mmol) by syringe, the reaction mixture was stirred and illuminated with visible light using a Xe light with an ultraviolet cut-off filter (>400 nm) for 24 h. The photocatalyst was recovered by centrifugation and filtration, and the filtrate was concentrated under reduced pressure. The product was isolated by flash chromatography on silica gel from the crude mixture.

For the reactions catalysed by free ligands, the specified amounts of corresponding photocatalysts were used instead of Zn–**BCTA**.

Results and discussion

Different numbers of thiophene moieties were inserted into the scaffold of H_3**TCA**, as demonstrated in Scheme 1b, then the triphenylamine-based ligands decorated with different numbers of thiophenes were subjected to examination of their photoelectronic properties. As shown in Fig. 1a, the UV-visible absorption spectra of H_3**MCTA** (mono[4-(5-carboxy-2-thienyl)phenyl]bis(4-carboxyphenyl)amine, **1**), H_3**BCTA** (bis[4-(5-carboxy-2-thienyl)-phenyl](4-carboxyphenyl)amine, **2**), and H_3**TCTA** (tris[4-(5-carboxy-2-thienyl)phenyl]amine, **3**) showed sequentially increasing amounts of red-shift in comparison with that of H_3**TCA**, and ligands **2** and **3** bearing bis- and tris-thiophenes exhibited considerable absorptions above 400 nm although their λ_{max} was still located in the near UV area. The electrochemical measurements of **1** to **3** exhibited redox potentials at 1.12 V, 1.25 V, and 1.36 V (*vs.* SCE), respectively, assignable to the redox potentials of the radical cation/neutral couples of the substituted triphenylamine moieties (Fig. 1b and e), demonstrating the stronger oxidative ability of the corresponding radical cations of ligands

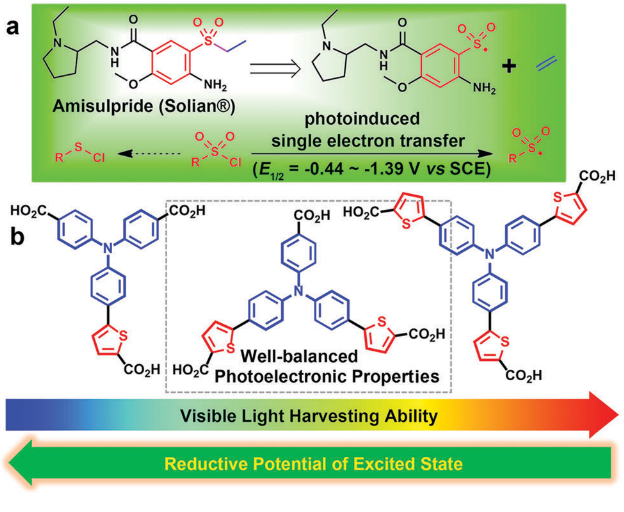

Scheme 1 Schematic illustration of ligand decoration for tuning the photoelectronic properties of the MOF to fulfill the demands for single-electron reduction of arylsulfonyl chlorides. (a) The possible construction of a bioactive aryl alkyl sulfone by sulfonyl radical addition onto alkenes (upper) and the electrochemical requirements for the photoreductive formation of sulfonyl radicals and the competitive pathway (lower). (b) Demonstration of iterative thiophene insertion for continuous modulation of the photoelectronic properties of triphenylamine-based ligands.

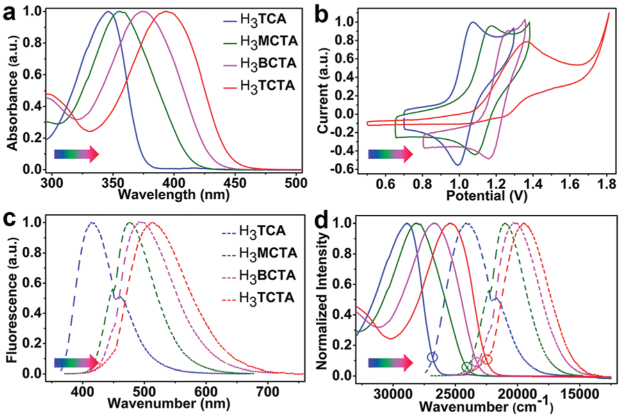

e

Ligand	λ_{max} (nm)	Ligand⁺/Ligand (V)	$E^{0\text{-}0}$ (eV)	Ligand⁺/Ligand* (V)
H_3TCA	346	1.03	3.32	-2.29
H_3MCTA	356	1.12	2.98	-1.86
H_3BCTA	375	1.25	2.88	-1.63
H_3TCTA	393	1.36	2.79	-1.43

Fig. 1 Photoelectronic properties of triphenylamine-based ligands decorated with different numbers of thiophenes. Comparisons of (a) UV-vis absorptions, (b) cyclic voltammograms (CVs), (c) fluorescence spectra, and (d) normalized absorption and emission spectra of H_3**TCA**, H_3**MCTA**, H_3**BCTA**, and H_3**TCTA**, respectively. The inserted arrows of (a) to (d) indicate the shifting directions of the peak signals of the corresponding photoelectronic properties. (e) Data sheet of the absorption maximum wavelengths (λ_{max}), the ground state oxidation potentials, the free energy changes (E^{0-0}) between the ground states and the vibrationally related excited states, and the reduction potentials of the excited states of H_3**TCA**, H_3**MCTA**, H_3**BCTA**, and H_3**TCTA**, respectively.

bearing more thiophene moieties. Then, the redox potentials of the excited-state ligand$^+$/ligand* couples were calculated to be the sequentially decreasing values −1.86 V, −1.63 V, and −1.43 V, respectively, on the basis of a free energy change (E^{0-0}) between the ground states and the vibrationally related excited states,[29] and the reduction potentials of those excited states seemingly fulfilled the demands for photoreducing a series of sulfonyl chlorides ($E_{1/2}$ = −0.44 to −1.39 V *vs.* SCE). However, the inter-ligand interactions within the MOFs generally led to variable degrees of energy loss of the excited states compared to those of the free ligands, making the reduction potentials of the excited states of the MOFs not as negative as those of the free ligands, while red-shifting the maximum absorption peaks in the case of the MOFs.[30] From consideration of the more and more enlarged π-systems from ligands **1** to **3**, the π–π interactions between the ligands and the concomitant weakening effect on the photoreducing abilities were estimated to be more and more significant,[31] which would suggest that the MOF constructed from H_3**TCTA** might not be competent at inducing photoreduction of sulfonyl chlorides with $E_{1/2}$ at the edge (*e.g.* −1.39 V *vs.* SCE).[32] To balance the trade-off between visible light harvesting ability and photoreduction ability of the modified ligands and the prospective MOFs, the bis-thiophene appended ligand H_3**BCTA** (**2**) was chosen as an ideal candidate owing to its well-balanced photoelectronic properties. We envisioned that the breaking of the C_3-symmetry of the triphenylamine-based ligand due to this bis-thiophene incorporation might distort the coordination geometry of the metal nodes within the MOF, possibly creating coordination vacancies for fixing substrates in close proximity to the photocatalytic centres.

The solvothermal reaction of H_3**BCTA** and $Zn(NO_3)_2\cdot 6H_2O$ in DMF at 100 °C for 3 days afforded a new coordination polymer Zn–**BCTA** in 65% yield. Elemental analysis (EA) and powder X-ray diffraction (PXRD) indicated that the bulk sample consisted of a pure phase (Fig. 6b). Thermogravimetric analysis (TGA) showed an impressive solvent loss of 55 weight percent (wt%) in the temperature range 20 to 190 °C, indicating an open framework structure (Fig. S5, ESI†). Single-crystal X-ray structural analysis revealed that this polymer crystallized in the monoclinic space group $C2/c$ (Table S1, ESI†). The asymmetric unit of Zn–**BCTA** contained a Zn_4O cluster, two **BCTA**$^{3-}$ moieties and two coordinated DMF molecules (Fig. S6, ESI†) and the framework formula was similar to that of the typical $Zn_4O(\mathbf{L})_3$ (**L** = tritopic ligand) of Zn(II)-MOFs bearing triangular linkers, for example, the well-known MOF-177.[33,34] In comparison to the octahedral $Zn_4O(CO_2)_6$ cluster of MOF-177 that was composed of four tetrahedrally coordinated Zn^{2+} ions, three Zn^{2+} ions (Zn1, Zn2 and Zn3) of Zn_4O node of Zn–**BCTA** also resided in tetrahedral environments, each coordinated by three carboxylate oxygen atoms from different **BCTA**$^{3-}$ moieties and a μ_4-O atom at the centre of the cluster. Meanwhile, the fourth Zn^{2+} (Zn4) ion adopted an octahedral coordination geometry surrounded by one μ_4-O atom, three oxygen atoms of different carboxylates, and other two carbonyl oxygen atoms from two coordinated DMF molecules. Each pair of adjacent Zn^{2+} ions of Zn_4O were bridged by a carboxylate group of ligand and the central μ_4-O bridge. Within the distorted Zn_4O tetrahedron around μ_4-O, the distances from μ_4-O to Zn ranged from 1.92 to 2.03 Å, and the Zn–Oμ_4–Zn angles were revealed to range from 108.1° to 112.1° and deviated slightly from the value for an ideal tetrahedron (Fig. 2a). Thus, the torsion of Zn_4O should be responsible for accommodating two additional DMF molecules besides six carboxylates. Moreover, it was believed that the coordinated DMF molecules were replaceable by coordinative organic solvents to expose the Lewis acidic coordination vacancies[35] as the active sites for the possible fixation and activation of substrates.

The tetranuclear Zn_4O clusters acted as 6-connected distorted octahedral secondary building units (SBUs), and the reduced-symmetry tripodal **BCTA**$^{3-}$ ligand rotated the arms with special angles to meet the requirements of the torsional octahedral geometries of the SBUs (Fig. 2b) and linked three Zn_4O clusters through the carboxylate groups to generate a 3D framework containing cavities with an opening diameter of *ca.* 22.2 Å (Fig. 2d). Different from the typical **pyr**,[36] **rtl**,[34] or **qom**[37] topologies of (6,3)-connected MOFs[38] constructed from octahedral $Zn_4O(CO_2)_6$ clusters and C_3-symmetric triangular linkers, structural analysis using the TOPOS program[39] indicated that Zn–**BCTA** could be represented as a 3,6-c net and **ant** topology with the Schläfli symbol $\{4^2;6\}_2\{4^4;6^2;8^8;10\}$, which could also be interpreted as the result of the deviation from C_3-symmetry of the modified ligand H_3**BCTA**. It should be noted that two independent networks are staggered to form a

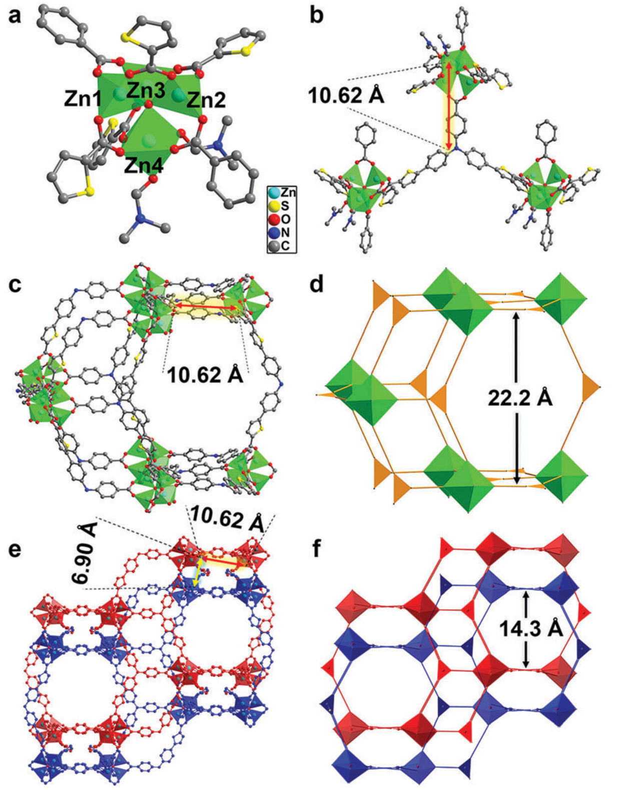

Fig. 2 Schematic illustration of the crystal structure of Zn–**BCTA**. The coordination environments of (a) the node (symmetry code: $1 + x$, $-y$, $0.5 + z$) and (b) the **BCTA**$^{3-}$ bridging ligand of Zn–**BCTA**. Ball-and-stick diagrams of the cage (c) before and (e) after interpenetration. Topological presentations of Zn–**BCTA** (d) before and (f) after interpenetration. Considering the Zn_4O SBUs as octahedrons and the **BCTA** crosslinker as triangles, the topology is **ant**.

two-fold interpenetrated 3D framework, with the opening diameter of the 1D channels reduced to *ca.* 14.3 Å (Fig. 2f). The interlocking and interweaving structures were envisioned to not only stabilize the crystalline solid during photocatalytic applications, but also to lead to closer proximity between the possibly fixed substrate and the photocatalytic centre to enhance the reaction efficiency (the nearest inter- *vs.* intra-network distances between the nitrogen centre of the **BCTA**$^{3-}$ moiety and the Zn^{2+} (Zn4) atom coordinated to DMF are 6.90 Å and 10.62 Å, respectively) (Fig. 2b, c and e). Moreover, the interpenetration resulting in denser distribution of chromophores was believed to interfere with the energy levels of the excited states, providing further modulation of the photoelectronic performance of the MOF.[30]

The free volume in fully desolvated Zn–**BCTA** was estimated to be approximately 67.9% using PLATON software.[28] Simultaneously, a methylene blue dye uptake experiment with Zn–**BCTA** was used to demonstrate the guest accessibility,[40] and the experiment yielded a methylene blue (MB) dye uptake amount of *ca.* 52% of the catalyst weight, as determined from the UV-vis spectra (Fig. 3a). Confocal laser scanning microscopy of the crystals soaked with MB gave a strong fluorescence response that can be assigned to the emission of MB (Fig. 3b), confirming the successful uptake of the dye molecules inside the crystals of the MOF.[41] The results implied the ability of Zn–**BCTA** to adsorb organic substrates within its open channels.

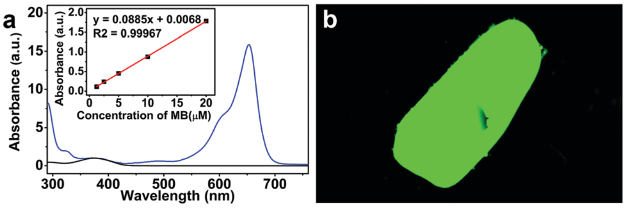

Fig. 3 Characterization of the accessible porosity of Zn–**BCTA**. (a) UV-vis measurements of methylene blue dye released from Zn–**BCTA** (blue: digested sample of Zn–**BCTA** soaked with MB; black: digested sample of Zn–**BCTA**), and (inset) the standard linear relationship between the absorption and the concentration. (b) Confocal image of a Zn–**BCTA** crystal soaked with MB.

The solid UV-vis absorption spectrum of solid-state Zn–**BCTA** exhibited a remarkable red-shift (λ_{max} = 416 nm) and stronger absorption in the visible light region (400 nm to 500 nm) in comparison to that of the H_3**TCA** based MOF-150,[21] indicating the superior visible light harvesting ability for practical applications (Fig. 4a). Solid-state electrochemical measurements revealed a redox potential of 1.08 V (*vs.* SCE) assignable to the Zn–**BCTA**$^+$/Zn–**BCTA** couple (Fig. 4b). In addition, the redox potential of the excited-state Zn–**BCTA**$^+$/Zn–**BCTA*** couple was calculated to be −1.49 V on the basis of a free energy change (E^{0-0}) between the ground state and the vibrationally related excited state of 2.57 eV (Fig. 4d). In comparison to MOF-150,[20] Zn–**BCTA** exhibited a much milder but still competent ability to photoreduce sulfonyl chlorides for the formation of sulfonyl radicals (−1.49 V of Zn–**BCTA** *vs.* −2.09 V of MOF-150[21]), and meanwhile avoided the competitive pathways under over-negative electronic potentials. The quenched luminescence (Fig. 5a) and the substantially decreased fluorescence lifetime (3.32 ns to 1.12 ns) (Fig. 5b) of the Zn–**BCTA** suspension upon addition of *p*-toluenesulfonyl chloride (TsCl) indicated a classical photoinduced electron transfer (PET) process from the excited

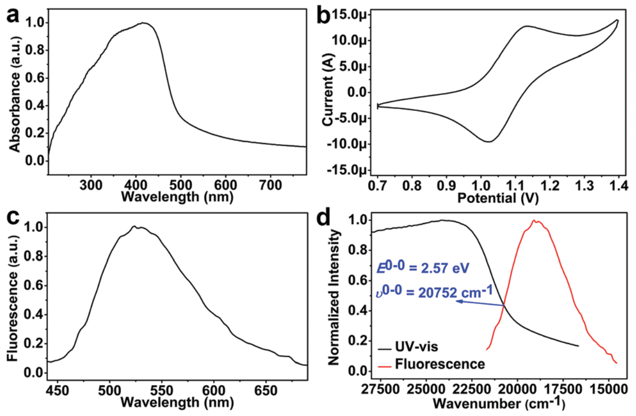

Fig. 4 Characterization of the photoelectronic properties of Zn–**BCTA**. (a) Solid-state UV-vis absorption spectra. (b) CVs. (c) Solid-state fluorescence. (d) Normalized absorption and emission spectra.

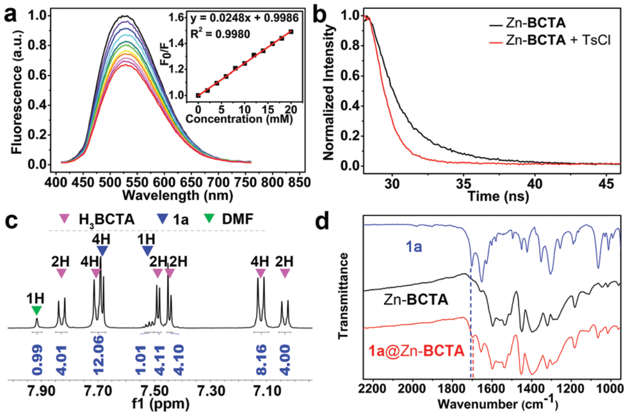

Fig. 5 Characterization of host–guest behavior between the framework of Zn–**BCTA** and the substrate or reagent. (a) Fluorescence spectra of Zn–**BCTA** upon the addition of TsCl and the corresponding simulated Stern–Volmer curve (inset). (b) The decreased fluorescence lifetime of the Zn–**BCTA** suspension upon addition of TsCl. (c) ^{1}H NMR spectrum of the crystals of **1a**@Zn–**BCTA** (digested in DMSO-d_6/DCl). The peaks marked with inverted blue triangles represent the aromatic signals of the encapsulated substrate **1a**. (d) Comparison of the infrared (IR) spectra of **1a** (blue line), Zn–**BCTA** (black line), and **1a**@Zn–**TCTA** (red line). The inserted dashed lines indicate the carbonyl peaks of **1a** molecules in the corresponding cases.

state of the **BCTA**$^{3-}$ moiety to TsCl, which directly yielded active toluenesulfonyl radicals.

Isoquinolinedione[42,43] and oxindole[44,45] moieties widely exist in natural products and pharmaceuticals and show certain biological activities. However, considering the importance of aryl alkyl sulfones in pharmaceutical fields, it would be interesting to merge an aryl alkyl sulfone and isoquinolinedione/oxindole within one motif to offer more possibility for drug development. Thus, the photocatalytic preparation of arylsulfonyl isoquinolinediones/oxindoles was chosen as the model reaction.[46,47] The initial exploration toward this tandem sulfonyl radical addition–cyclisation process was carried out with *N*-methacryloyl-*N*-methylbenzamide **1a** (0.25 mmol, 1.0 equiv.) as the substrate, TsCl **2a** (0.50 mmol, 2.0 equiv.) as the arylsulfonyl radical source, 2,4,6-collidine (0.50 mmol, 2.0 equiv.) as the additive base, and with a 2.5 mol% loading amount of Zn–**BCTA** in 1,2-dichloroethane (DCE) at room temperature, using a Xe light with an ultraviolet cut-off filter (>400 nm) as the visible light source. The target compound **3a** was obtained only in a 15% isolated yield after 24 h of reaction (Table 1, entry 1). Low conversion was also observed in the cases using other uncoordinated solvents like toluene (entry 2). Then, some coordinated solvents such as tetrahydrofuran (THF), ethyl acetate (EtOAc), and especially acetonitrile (MeCN) were found to be capable of improving the conversion (entries 3 to 5). According to the report of Jeong and coworkers,[48] it has been concluded that coordinative solvents can enhance the dissociation of the coordinated DMF molecules from the zinc nodes, thus providing more coordination vacancies for fixing the substrates. Then, different loading amounts of the photocatalyst were examined, and 2.5 mol% of Zn–**BCTA** was proven to be more practical (entries 5 to 7). Furthermore, screening different loading amounts of TsCl and collidine revealed the necessity of using 2.0 equiv. of the radical source and additive base, and either decreased or increased amounts led to lower yields (entries 8 and 9). The optimal reaction conditions are shown in entry 5. The following control experiments demonstrated that the integrity of the photocatalyst, visible light irradiation, and an inert gas atmosphere were indispensable factors in this reaction (entries 10, 11, 14 to 17). No desired product was found in the presence of 1.2 equiv. of the radical scavenger TEMPO (2,2,6,6-tetramethyl-1-piperidinyloxy), demonstrating a radical mechanism (entry 19). On the other hand, a comparison of the photocatalytic performances of free ligands bearing different numbers of thiophenes further demonstrated the well-balanced reactivity of the two thiophene incorporated ligand (entries 11 to 13). Removal of MOF solids by hot-filtration after 3 h shut down the reaction immediately (Table 1, entry 18), which suggested the heterogeneous nature of this reaction. After the reaction, the MOF Zn–**BCTA** could be easily recovered by simple filtration, and then reused for at least 3 cycles without any remarkable deterioration in activity (Fig. 6a). The fact that the X-ray powder diffraction (XRD) patterns of the photocatalyst samples before and after the reactions did not significantly change indicated the maintaining of the corresponding crystallinity of Zn–**BCTA** (Fig. 6b).

Then, we investigated the host–guest interactions between the framework of Zn–**BCTA** and the substrate by soaking the crystals in an acetonitrile solution containing **1a**. ^{1}H NMR analysis of the digested crystals revealed that Zn–**BCTA** could adsorb approximately 1.0 equivalent of **1a** per Zn_4O SBU (Fig. 5c). The infrared (IR) spectrum of the **1a**-impregnated crystals exhibited a 7 cm^{-1} red-shift (1701 cm^{-1} to 1694 cm^{-1}) in the carbonyl stretching vibrations of **1a** (Fig. 5d), indicating the fixation of **1a** by coordination with its carbonyl group and activation of its unsaturated alkene moiety. Simultaneously, it was found that one of the two coordinated DMF molecules was replaced by **1a** (Fig. 5c), demonstrating the feasibility of acetonitrile assisted activation of this MOF and also implying the role of the coordination vacancy as the active site. However, the quality of the **1a**-impregnated crystal **1a**@Zn–**BCTA** was not sufficient for single crystal X-ray diffraction analysis.[49,50]

This heterogeneous photocatalytic approach was extended to the tandem sulfonylation–cyclisation of a series of *N*-aryl-methacrylamides and *N*-aroyl-methacrylamides, leading to the formation of the corresponding arylsulfonyl isoquinolinediones/oxindoles in moderate to high yields as shown in Table 2. When substrates bearing *meta*-substituted aryl moieties were used, only one type of regioisomer was obtained, indicating the high regioselectivities of the reactions (Table 2, **3b** and **3f**).[51] Stereoselective photoredox catalysis has long been hindered due to the dearth of stereocontrol strategies in radical processes,[52–54] especially in the case of there being no covalent or ionic binding sites in the substrates.[55] The possibility of an existing carbonyl–zinc node interaction encouraged us to explore the stereocontrol effect of the local confined environment on this photocatalytic tandem process. The sulfonylation–cyclisation of vicinal di-substituted electron-deficient olefin **1g** and **1h**

Table 1 Optimization of the reaction conditions and control experiments[a]

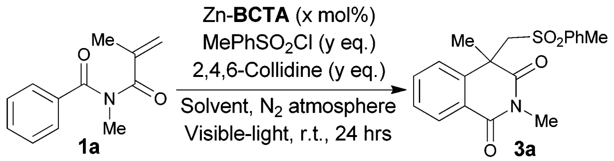

Entry	Catalyst (mol%)	Solvent	TsCl/collidine (x equiv.)	Yield[b] (%)
1	Zn–**BCTA** (2.5)	DCE	2	15
2	Zn–**BCTA** (2.5)	$PhCH_3$	2	<10
3	Zn–**BCTA** (2.5)	THF	2	27
4	Zn–**BCTA** (2.5)	EtOAc	2	48
5	***Zn–BCTA (2.5)***	***CH_3CN***	***2***	***85***
6	Zn–**BCTA** (1.25)	CH_3CN	2	55
7	Zn–**BCTA** (5)	CH_3CN	2	86
8	Zn–**BCTA** (2.5)	CH_3CN	1.2	64
9	Zn–**BCTA** (2.5)	CH_3CN	3	76

Entry	Variants of the optimal conditions	Yield[b] (%)
10	$Zn(NO_3)_2·6H_2O$ (5)	Trace
11	H_3**BCTA** (2.5)	39
12	H_3**MCTA** (2.5)	17
13	H_3**TCTA** (2.5)	26
14	$Zn(NO_3)_2·6H_2O$ (5) + H_3**BCTA** (2.5)	45
15	No photocatalyst	Trace
16	Under darkness	0
17	Air conditions	0
18	3 h first with Zn–**BCTA** (2.5), then remove the catalyst	51
19	With TEMPO (1.2 equiv.) added	0

[a] Reaction conditions: **1a** (0.25 mmol, 1.0 equiv.), *p*-toluenesulfonyl chloride **2a** and additive base 2,4,6-collidine (specified amounts), photocatalyst (specified amount calculated based on the **BCTA** moiety), degassed solvent (1.0 mL), room temperature (r.t.) and an N_2 atmosphere, 24 h. [b] Isolated yields.

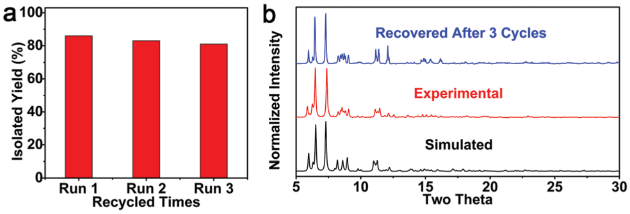

Fig. 6 (a) Histograms of reusing experiments of the MOF Zn–**BCTA**. (b) X-ray powder diffraction (XRD) patterns of freshly prepared Zn–**BCTA** (middle), the recycled catalyst after 3 runs (up), and its simulated pattern based on the reported single-crystal data (bottom).

afforded the products in the yields 63% and 61%, respectively, with diastereoselectivities higher than 95 : 5 (**3g** and **3h**).[32] In comparison, the use of a free ligand as the catalyst in a homogeneous control reaction gave diminished conversion and inferior diastereoselectivity (Table 2, **3g**).

As expected, a series of arylsulfonyl chlorides, for which the reduction potentials of the excited states covered a wide range, were proven to be applicable to this heterogeneous photocatalytic approach (Table 3). Arylsulfonyl chlorides bearing electron-donating (MeO-, **2e**) or electron-withdrawing (F-, **2c**; Br-, **2d**) substituents on the benzene ring could be transformed into the corresponding desired products efficiently in good yields (Table 3, **3j** to **3l**). Other carbocycle and heterocycle bearing arylsulfonyl radical sources like naphthalene-1-sulfonyl

Table 2 Investigations on the substrate scope of the activated alkenes[a]

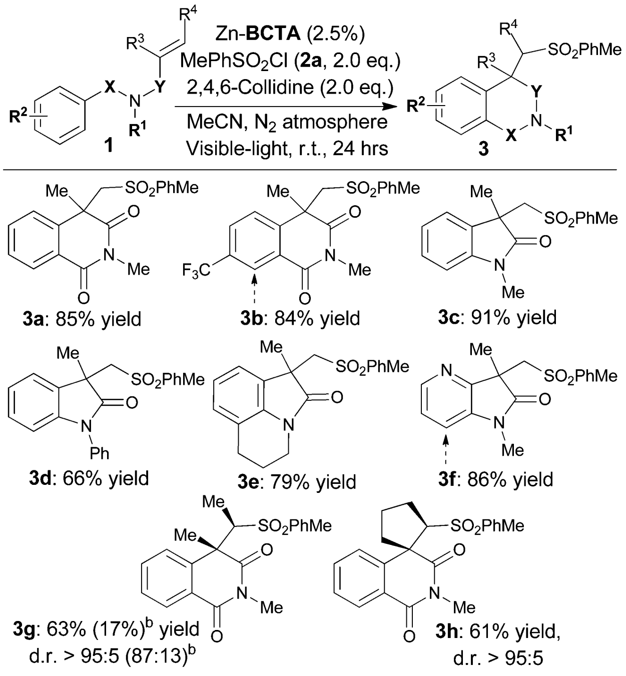

[a] Optimal reaction conditions as shown in Table 1, entry 5; isolated yields. Diastereoselectivity (diastereomeric ratio, d.r.) was determined through ^1H NMR of the crude products. [b] Free ligand H_3**BCTA** was used as the photocatalyst.

Table 3 Investigations on the substrate scope of the sulfonyl chlorides[a]

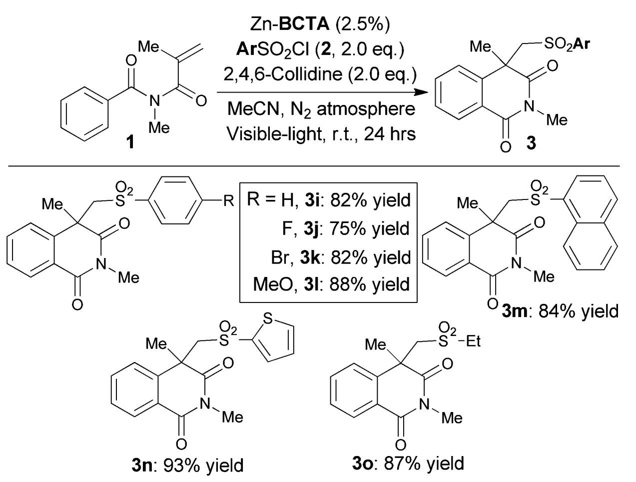

[a] Optimal reaction conditions as shown in Table 1, entry 5; isolated yields.

chloride (**2f**) and thiophene-2-sulfonyl chloride (**2g**) afforded the target compounds in the yields 84% and 93%, respectively (**3m** and **3n**). More noticeably, the aliphatic derivative ethanesulfonyl chloride (**2h**) for which the oxidation potential should be comparable to that of methanesulfonyl chloride (MsCl, $E_{1/2} = -1.39$ V), was also amenable to this photocatalytic system to give the corresponding product **3o** in 87% yield.

Based on the above results and previous related reports, a possible reaction mechanism was proposed as outlined in Scheme 2. First, MeCN assisted the dissociation of the coordinated DMF on the nodes to create coordination vacancies (Scheme 2, a) for fixing the substrate by coordinating to the carbonyl group and drawing the substrate closer towards the spatially neighboring photocatalytic centre. Upon irradiation with visible light, the excited state of the $\mathbf{BCTA}^{3-}$ moiety transferred an electron to the arylsulfonyl chloride for the generation of an arylsulfonyl radical (Scheme 2, b).[56] The addition of the sulfonyl radical to the carbon–carbon double bond[57] of **1a** and the following intramolecular addition[58,59] to the aromatic ring furnished the cyclic radical intermediate **A** (Scheme 2, c). After oxidation by the cation radical form of the nitrogen centre of $\mathbf{BCTA}^{3-}$, intermediate **A** was transformed into the corresponding cation **B** with the regeneration of the photocatalytic centre (Scheme 2, d). Finally, the deprotonation of **B** assisted by the additive base yielded the desired product **3a.** It was speculated that the spatial proximity of the docked substrate toward the photocatalytic centre within this interpenetrated framework facilitated the photoredox process,[60] and the crowded local environment might impose a spatial confined effect[61–64] onto the fixed substrate for premium diastereocontrol of the reaction.

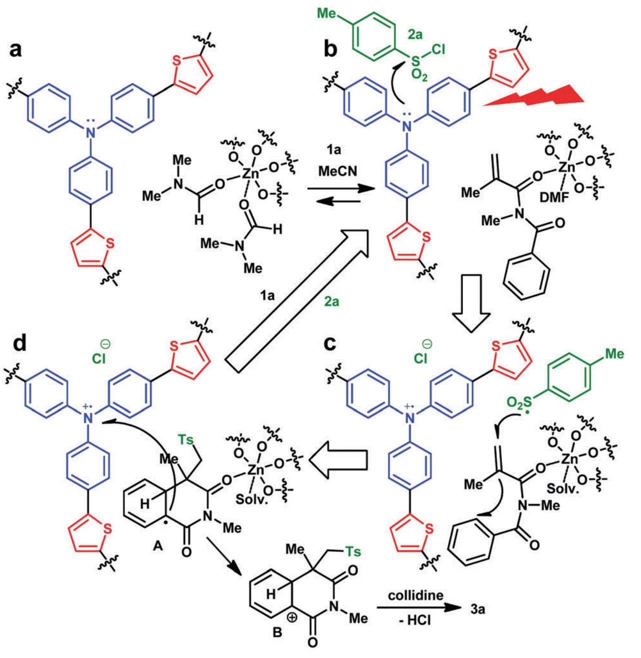

Scheme 2 Schematic illustration of the mechanistic view of this reaction.

Conclusions

In this study, a ligand engineering strategy of inserting thiophenes into the scaffold of triphenylamine-based ligands was developed as a powerful tool for red-shifting the UV-vis absorption peaks, improving the oxidation potentials of the ground states, and decreasing the reduction potentials of the excited states of the ligands and the MOFs. Thus, it allowed one to precisely and continuously tune the photoelectronic properties of MOF-based photocatalysts according to specific demands. In the case study of the photocatalytic preparation of bio-interesting sulfonyl isoquinolinediones/oxindoles, a ligand decorated with two thiophenes was chosen as the candidate, resulting in a good visible light-harvesting ability and a suitable excited-state redox potential of the corresponding MOF Zn–**BCTA** that fulfilled the requirements for photoineduced generation of sulfonyl radicals while circumventing the competitive over-reduction of sulfonyl moieties. The deviation from C_3-symmetry of the modified ligand forged a distortion of the Zn_4O nodes to provide potential sites for harnessing substrates. Moreover, the interpenetrated frameworks facilitated docking of the substrate in closer proximity to the photoredox-active centre. As a result, this heterogeneous photocatalytic system exhibited superior efficiency and diastereocontrol to its homogeneous counterpart using a free ligand. Currently, further extension of this ligand engineering strategy is being extensively studied in our lab for designing MOF-based photocatalytic systems from the perspective of pharmaceutical/fine chemical orientation.

Author contributions

T. Zhang and C. Duan conceived the project. T. Zhang designed the experiments and wrote the manuscript. T. Zhang, Y. Shi, S. Zhang, and C. Jia performed the experiments. Y. Shi and C. He solved and refined the X-ray crystal structures. All the authors discussed the results and commented on the manuscript.

Conflicts of interest

There are no conflicts of interest to declare.

Acknowledgements

We gratefully acknowledge the financial support for this work from the National Natural Science Foundation of China (21402020, U1608224, and 21531001), the Fundamental Research Funds for the Central Universities (DUT16RC(4)09 and DUT18LK50), and the 111 Project (B16008).

Notes and references

1 N. S. Simpkins, *Sulfones in Organic Synthesis*, ed. J. E. Baldwin, Pergamon Press, Oxford, 1993.
2 R. Patel, T. W. Packham, A. L. Germain, J. R. Barras and D. J. Milne, WO9507877 19950323, 1995.
3 D. J. Paghdar, M. R. Kolekar, T. N. Deshpande, S. P. Patil, Y. A. Chavan, P. C. Ray and G. P. Singh, WO2011158084 A1 20111222, 2011.
4 C. M. M. da Silva Corrêa, M. D. C. M. Fleming, M. A. B. C. S. Oliveira and E. M. J. Garrido, *J. Chem. Soc., Perkin Trans. 2*, 1994, 1993–2000.
5 C.-J. Wallentin, J. D. Nguyen, P. Finkbeiner and C. R. J. Stephenson, *J. Am. Chem. Soc.*, 2012, **134**, 8875–8884.
6 H. Jiang, X. Chen, Y. Zhang and S. Yu, *Adv. Synth. Catal.*, 2013, **355**, 809–813.
7 S. K. Pagire, S. Paria and O. Reiser, *Org. Lett.*, 2016, **18**, 2106–2109.
8 N. Koichi, M. Takashi and H. Satoshi, *Chem. Lett.*, 1994, 1705–1708.
9 A. Houmam and E. M. Hamed, *Phys. Chem. Chem. Phys.*, 2012, **14**, 113–124.
10 S. K. Pagire, A. Hossain and O. Reiser, *Org. Lett.*, 2018, **20**, 648–651.
11 M. Chen, Z.-T. Huang and Q.-Y. Zheng, *Chem. Commun.*, 2012, **48**, 11686.
12 M. Peplow, *Nature*, 2015, **520**, 148–150.
13 A. G. Slater and A. I. Cooper, *Science*, 2015, **348**, 988.
14 T. Zhang and W. Lin, *Chem. Soc. Rev.*, 2014, **43**, 5982–5993.
15 S. Wang and X. Wang, *Small*, 2015, **11**, 3097–3112.
16 A. Dhakshinamoorthy, A. M. Asiri and H. García, *Angew. Chem., Int. Ed.*, 2016, **55**, 5414–5445.
17 L. Zeng, X. Guo, C. He and C. Duan, *ACS Catal.*, 2016, **6**, 7935–7947.
18 M. Usman, S. Mendiratta and K.-L. Lu, *Adv. Mater.*, 2017, **29**, 1605071.
19 P. Sippel, D. Denysenko, A. Loidl, P. Lunkenheimer, G. Sastre and D. Volkmer, *Adv. Funct. Mater.*, 2014, **24**, 3885–3896.
20 H. K. Chae, J. Kim, O. D. Friedrichs, M. O. Keeffe and O. M. Yaghi, *Angew. Chem., Int. Ed.*, 2003, **42**, 3907–3909.
21 P. Wu, C. He, J. Wang, X. Peng, X. Li, Y. An and C. Duan, *J. Am. Chem. Soc.*, 2012, **134**, 14991–14999.
22 M. W. Logan, S. Ayad, J. D. Adamson, T. Dilbeck, K. Hanson and F. J. Uribe-Romo, *J. Mater. Chem. A*, 2017, **5**, 11854–11863.
23 X. Guo, L. Zeng, Z. Wang, T. Zhang, C. He and C. Duan, *RSC Adv.*, 2017, **7**, 52907–52913.
24 SMART, *Data collection software (version 5.629)*, Bruker AXS Inc., Madison, WI, 2003.
25 SAINT, *Data reduction software (version 6.45)*, Bruker AXS Inc., Madison, WI, 2003.
26 G. M. Sheldrick, *Acta Crystallogr., Sect. C: Struct. Chem.*, 2015, **71**, 3–8.
27 P. V. D. Sluis and A. L. Spek, *Acta Crystallogr.*, 1990, **46**, 194–201.
28 A. L. Spek, *PLATON99, A Multipurpose Crystallographic Tool*, Utrecht University, Utrecht, The Netherlands, 1999.
29 G. J. Kavarnos, *Fundamentals of Photoinduced Electron Transfer*, VCH, New York, 1993.
30 P. Deria, J. Yu, T. Smith and R. P. Balaraman, *J. Am. Chem. Soc.*, 2017, **139**, 5973–5983.
31 J. Yu, J. Park, A. Van Wyk, G. Rumbles and P. Deria, *J. Am. Chem. Soc.*, 2018, **140**, 10488–10496.
32 T. Zhang, X. Guo, Y. Shi, C. He and C. Duan, *Nat. Commun.*, 2018, **9**, 4024.
33 H. K. Chae, D. Y. Siberio-Pérez, J. Kim, Y. Go, M. Eddaoudi, A. J. Matzger, M. O'Keeffe and O. M. Yaghi, *Nature*, 2004, **427**, 523–527.
34 Y.-B. Zhang, H. Furukawa, N. Ko, W. Nie, H. J. Park, S. Okajima, K. E. Cordova, H. Deng, J. Kim and O. M. Yaghi, *J. Am. Chem. Soc.*, 2015, **137**, 2641–2650.
35 J. Bae, E. J. Lee and N. C. Jeong, *Chem. Commun.*, 2018, **54**, 6458–6471.
36 H. K. Chae, J. Kim, O. D. Friedrichs, M. O'Keeffe and O. M. Yaghi, *Angew. Chem.*, 2003, **115**, 4037–4039.
37 H. Furukawa, N. Ko, Y. B. Go, N. Aratani, S. B. Choi, E. Choi, A. Ö. Yazaydin, R. Q. Snurr, M. O'Keeffe, J. Kim and O. M. Yaghi, *Science*, 2010, **329**, 424–428.
38 M. O'Keeffe and O. M. Yaghi, *Chem. Rev.*, 2012, **112**, 675–702.
39 V. A. Blatov, A. P. Shevchenko and D. M. Proserpio, *Cryst. Growth Des.*, 2014, **14**, 3576–3586.
40 L. Ma, J. M. Falkowski, C. Abney and W. Lin, *Nat. Chem.*, 2010, **2**, 838–846.
41 S. M. Shin, M. S. Lee, J. H. Han and N. Jeong, *Chem. Commun.*, 2014, **50**, 289–291.
42 M. Billamboz, F. Bailly, C. Lion, N. Touati, H. Vezin, C. Calmels, M. Andréola, F. Christ, Z. Debyser and P. Cotelle, *J. Med. Chem.*, 2011, **54**, 1812–1824.
43 S. K. V. Vernekar, Z. Liu, E. Nagy, L. Miller, K. A. Kirby, D. J. Wilson, J. Kankanala, S. T. Sarafianos, M. A. Parniak and Z. Wang, *J. Med. Chem.*, 2015, **58**, 651–664.
44 B. S. Jensen, *CNS Drug Rev.*, 2002, **8**, 353–360.
45 C. V. Galliford and K. A. Scheidt, *Angew. Chem., Int. Ed.*, 2007, **46**, 8748–8758.
46 X. Liu, T. Cong, P. Liu and P. Sun, *Org. Biomol. Chem.*, 2016, **14**, 9416–9422.
47 X.-F. Xia, S.-L. Zhu, D. Wang and Y.-M. Liang, *Adv. Synth. Catal.*, 2016, **358**, 859–865.
48 J. Bae, E. J. Lee and N. C. Jeong, *Chem. Commun.*, 2018, **54**, 6458–6471.

49 Y. Inokuma, S. Yoshioka, J. Ariyoshi, T. Arai, Y. Hitora, K. Takada, S. Matsunaga, K. Rissanen and M. Fujita, *Nature*, 2013, **495**, 461–466.

50 X. Jing, C. He, D. Dong, L. Yang and C. Duan, *Angew. Chem., Int. Ed.*, 2012, **51**, 10127–10131.

51 W. Kong, M. Casimiro, N. Fuentes, E. Merino and C. Nevado, *Angew. Chem., Int. Ed.*, 2013, **52**, 13086–13090.

52 Y. Inoue, *Chem. Rev.*, 1992, **92**, 741–770.

53 D. A. Nicewicz and D. W. C. MacMillan, *Science*, 2008, **322**, 77–80.

54 J. Du, K. L. Skubi, D. M. Schultz and T. P. Yoon, *Science*, 2014, **344**, 392–396.

55 M. P. Sibi, J. Ji, J. B. Sausker and C. P. Jasperse, *J. Am. Chem. Soc.*, 1999, **121**, 7517–7526.

56 M. Tamba, K. Dajka, C. Ferreri, K.-D. Asmus and C. Chatgilialoglu, *J. Am. Chem. Soc.*, 2007, **129**, 8716–8723.

57 A. Wimmer and B. König, *Beilstein J. Org. Chem.*, 2018, **14**, 54–83.

58 T. Shen, Y. Yuan, S. Song and N. Jiao, *Chem. Commun.*, 2014, **50**, 4115–4118.

59 W. Yang, S. Yang, P. Li and L. Wang, *Chem. Commun.*, 2015, **51**, 7520–7523.

60 Z. Xia, C. He, X. Wang and C. Duan, *Nat. Commun.*, 2017, **8**, 361.

61 M. Yoshizawa, M. Tamura and M. Fujita, *Science*, 2006, **312**, 251–254.

62 M. Yoshizawa, Y. Takeyama, T. Kusukawa and M. Fujita, *Angew. Chem., Int. Ed.*, 2002, **41**, 1347–1349.

63 Y. Nishioka, T. Yamaguchi, M. Kawano and M. Fujita, *J. Am. Chem. Soc.*, 2008, **130**, 8160–8161.

64 B. Qi, T. Zhang, M. Li, C. He and C. Duan, *Catal. Sci. Technol.*, 2017, **7**, 5872–5881.